Matter

CellPress
OPEN ACCESS

Article

# A fluidic relaxation oscillator for reprogrammable sequential actuation in soft robots

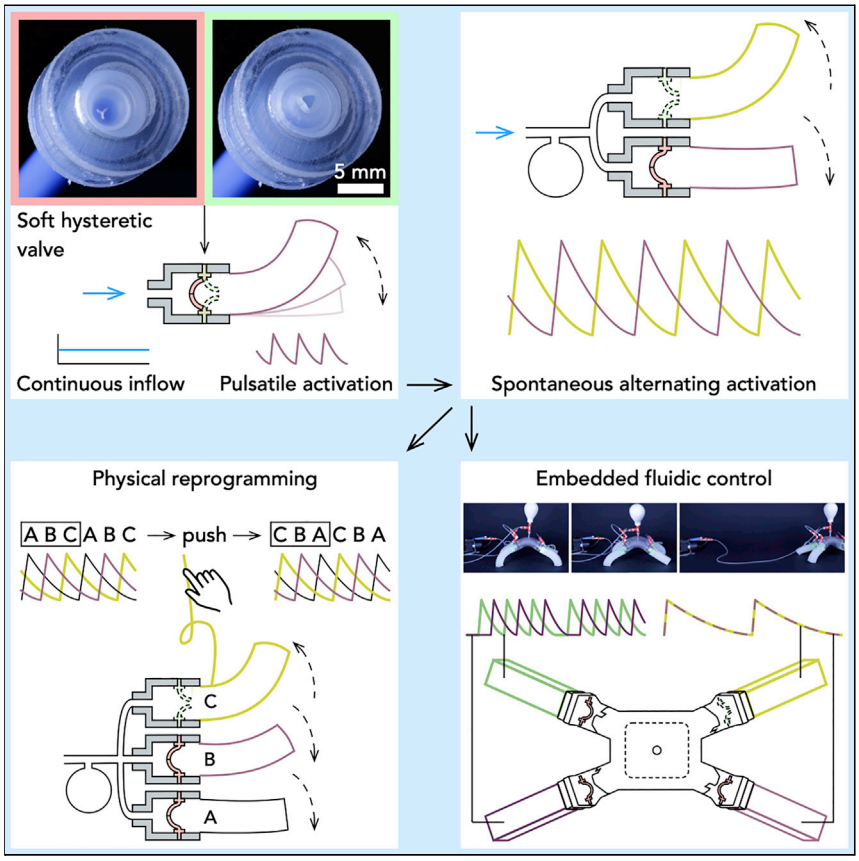


In the field of soft robotics, a long-term goal is the creation of responsive systems, for applications such as controlled drug release or autonomous exploration of unknown terrain. We introduce a compact soft valve that transforms a continuous flow of air into timed pulses, and we show that multiple such valves can be arranged in fluidic circuits to create responsive soft robots.

Lucas C. van Laake, Jelle de Vries, Sevda Malek Kani, Johannes T.B. Overvelde

overvelde@amolf.nl

## Highlights

A simple, compact elastomeric valve is used to control soft-robotic actuators

Up to five actuators are activated in different patterns

The pattern can be changed on the fly by mechanical reprogramming

We demonstrate a four-legged robot that requires nothing but a pump to walk

**Benchmark**
First qualification/assessment of material properties and/or performance

van Laake et al., Matter 5, 1–20
September 7, 2022 
Published by Elsevier Inc.
https://doi.org/10.1016/j.matt.2022.06.002

Please cite this article in press as: van Laake et al., A fluidic relaxation oscillator for reprogrammable sequential actuation in soft robots, Matter (2022), https://doi.org/10.1016/j.matt.2022.06.002

Matter

CellPress
OPEN ACCESS

Article

# A fluidic relaxation oscillator for reprogrammable sequential actuation in soft robots

Lucas C. van Laake,[1] Jelle de Vries,[1] Sevda Malek Kani,[1] and Johannes T.B. Overvelde[1,2,3,*]

## SUMMARY

**Despite exciting developments in soft robotics, fully autonomous systems remain elusive. Fluidic circuits could enable fully embedded control of soft robots without using electronics. In this work, we introduce a simple and compact soft valve with intentional hysteresis, analogous to an electronic relaxation oscillator. By integrating the valve with a soft actuator, we transform a continuous inflow to cyclic activation. Importantly, we show that our circuits can activate up to five actuators in various sequences and that we can physically reprogram the activation order by varying the (initial) conditions in the fluidic circuit. Moreover, we show the feasibility of our approach under more realistic conditions by building a four-legged robot. Our work paves the way toward fully autonomous soft robots that can interact with their environment to reprogram their behavior, e.g., to trigger targeted drug release inside our body or to change gait to move past obstacles.**

## INTRODUCTION

Soft robots are compliant enough to be deformed by interactions with their environment while being stiff enough to perform meaningful action. Prime examples of soft robots are starfish-like grippers that are soft enough to wrap around an object without knowing its shape yet strong enough to lift significant weight.[1] Similar robotic systems can also achieve locomotion, enabling soft walking robots that require less control to navigate unknown terrain than traditional rigid robots.[2] While soft robots have found real-world adoption as end effectors on robotic arms for pick-and-place applications[3] and have, for example, been applied for medical rehabilitation[4] and implants,[5] soft mobile robots remain elusive. This may be explained by the fact that locomotion requires the control of multiple actuators instead of a single stimulus to control the grasping motion of a soft gripper. In order to build fully soft-robotic systems that operate autonomously, we need to embody such robots with more intelligence by embedding computation.[6]

Typical fluidic actuators consist of a silicone matrix embedded with channels and chambers.[7–11] When subjected to a pressurized fluid, these actuators bend, extend, contract, or twist in order to make a robot walk,[8] jump,[12] or swim.[13] Importantly, for the robots to perform certain tasks, their individual limbs need to be activated in a specific sequence. The typical approach is to use one or more manually operated or motor-controlled syringes[14] or (electro-)mechanical valves.[4] Due to the weight of these rigid components, they are typically not placed on the robot, such that fluidic tethers are needed. Similarly, the tethers provide the ability to externally reprogram the actuation sequence when needed.

## Progress and potential

Soft robotics is an emerging research field fueled by a vision of adaptative behavior in unpredictable environments and safe cooperation with humans. Soft robots possess so-called embodied intelligence, for example, in soft grippers that conform to arbitrarily shaped objects. However, higher-level adaptivity remains elusive. To bring this goal a step closer to reality, we introduce a compact soft valve. Fluidic circuits with our valves transform a continuous flow of air into timed pulses that activate up to five actuators in different sequences. We can select which sequence is executed, and excitingly, the system can switch between sequences in response to a physical cue. We demonstrate real-life applicability by controlling a four-legged walker. As such, our work leads the way toward fully autonomous soft robots that interact with their environment, for example, triggering drug release inside our body or changing gait to move past obstacles, without any electronics.

Recently, efforts have been made to replace the electronic control using only fluidic elements. Making use of interactions between the mechanical and fluidic properties of actuators, valves, and channels, these methods point the way to autonomous soft robots with all of their intelligence embedded in their elastomeric bodies.[15,16] Analogously to electronics, in soft fluidic control, we can identify innovations on the component level as well as the circuit level, and it is clear that advances on both levels are needed to improve the complexity of the behavior that can be embodied in the soft robots. So far, mostly low-level functions have been demonstrated, where sequences of actions can be triggered in the robot by externally supplied time-varying pressure inputs. For example, sequential activation of soft fluidic actuators has been achieved by connecting actuators in series with tubes of optimized diameter and length.[17] Besides combining components with a linear response, a combination of actuators with a nonmonotonic pressure-volume relation can also be designed to actuate in a given sequence.[18,19] A combination of viscous friction and nonlinear actuators can be exploited for peristaltic motion[20] or to expand the number of possible state transitions.[21] Another example is so-called band-pass valves that let low flows through but block high flows, which allows setting the pressure of multiple actuators individually using a single time-controlled pressure source.[22] Finally, following design principles from digital electronics, fluidic transistors can be arranged to control grasping and locomotion states using three fluidic drive lines[23] or to control eight outputs from three inputs.[24]

The key limitation for all of the above-mentioned systems is that they rely on externally timed inputs and therefore require tethers to operate. To our knowledge, there are only two examples of untethered soft robots with fluidic embedded control, and both of these breakthrough results originate from their ability to generate timed signals on the robot itself. The first example is a three-dimensional (3D)-printed octopus-inspired robot that employs a micro-fluidic oscillator[25] to alternate between two groups of actuators.[15] The second untethered soft robot[16] uses soft ring oscillators[26] that, when provided with a constant pressure, generate cyclical, timed pressure signals to three different groups of actuator chambers each.[27] This control system implements a soft, bistable valve that can be used as a switch and for cyclic activation of a single actuator[28] or that can be used in digital logic circuits.[29]

In all these applications, cyclic and programmable activation of multiple actuators is key in moving toward autonomous behavior in soft robots. In the previous two examples of untethered robots, the employed oscillators have only been demonstrated to activate up to a maximum of three degrees of freedom each. More importantly, they fundamentally only support a single sequence, such that reprogramming the actuators' activation order requires "rewiring" of the system.[16] To overcome these limitations, in this work, we introduce an extremely simple design for a soft valve that can be directly integrated with soft actuators. In contrast to the straightforward design and fabrication, the behavior of the valve is highly nonlinear and shows mechanical and fluidic hysteresis, which we harness to activate and reprogram up to five actuators in sequences.

We first introduce the design of the valve and show it in its most basic arrangement where it forms a single relaxation oscillator. The valve oscillates under continuous inflow of air, such that no external timing is required. We show that this oscillator can be used to cyclically activate a soft bending actuator placed behind the valve. We then connect two valves and actuators in parallel and analyze an instability that leads to alternating activation of the two actuators. Supported by a model

[1]Autonomous Matter Department, AMOLF, Science Park 104, 1098 XG Amsterdam, the Netherlands

[2]Institute for Complex Molecular Systems and Department of Mechanical Engineering, Eindhoven University of Technology, P.O. Box 513, 5600 MB Eindhoven, the Netherlands

[3]Lead contact

*Correspondence: overvelde@amolf.nl

https://doi.org/10.1016/j.matt.2022.06.002

Please cite this article in press as: van Laake et al., A fluidic relaxation oscillator for reprogrammable sequential actuation in soft robots, Matter (2022), https://doi.org/10.1016/j.matt.2022.06.002





that describes fluidic circuits including multiple valves in parallel, we experimentally demonstrate a novel way to control the sequence and timing of up to five actuators. This number is limited by imperfections due to production tolerances, and we show how the allowed imperfection level scales with the number of degrees of freedom. Moreover, we show that the fluidic circuit can repeatedly change its sequence of activation in response to an external stimulus. Finally, we show that we can directly integrate a fluidic control system into a soft robot and demonstrate our approach under more realistic conditions. As such, our proposed fluidic relaxation oscillator enables new kinds of medical and mobile robotics applications and brings the concept of fully autonomous soft robotics a step closer to realization.

## RESULTS

### Transforming a continuous flow into pulses

With the aim of building a soft fluidic control system for soft robots, we start by developing a fluidic relaxation oscillator that transforms a continuous flow into a pulsatile flow. We do so by fabricating an elastic valve (Figure 1A), which is placed directly in a fluid flow. The valve consists of a curved membrane that contains three slits that meet at its apex. In this work, we use valves with thickness $T = 0.75$ mm, angle $\theta = 75°$, radius $a_0 = 2.5$ mm, and the slits have length $L = 0.75$ mm (Figure 1B). These values result in $\Delta p_{open} \approx 60$ kPa, $\Delta p_{close} \approx 5$ kPa, and $R_{open} \approx 2$ kPa/ standard liter per minute (SLPM). The valve is fabricated by casting a silicone elastomer (Dragon Skin 20, Smooth-On) in a 3D-printed mold, after which the slits are machined using a laser cutter. It is then placed in a 3D-printed holder to create a robust, self-contained unit (Figure 1B; experimental procedures).

Importantly, the membrane exhibits a mechanical instability that translates into fluidic hysteresis (Figure 1C). Upon applying an increasing pressure to the curved membrane, it will undergo several stages, as shown in Figure 1D. (1) For very low pressures, the valve is not completely closed due to the finite width of the laser-cut slits, and some fluid can flow through the opening. (2) An increasing pressure closes the slits, such that no fluid can pass through the valve. (3) Upon reaching a critical pressure difference $\Delta p_{open}$, the curved membrane snaps to an inverted state, opening the slits and letting fluid through. In this open state, the valve acts as a flow restriction. (4) Importantly, when decreasing the pressure, the membrane does not snap back at the same point, and instead, (5) the valve closes at a lower pressure difference $\Delta p_{close}$.

Next, we apply a continuous air inflow $Q = 1$ SLPM to the valve and measure pressure before, as well as flow rate through, the valve. Interestingly, we observe that a system containing only the valve transforms a continuous inflow into a pulsatile outflow (Figures 1E and 1G; Video S1). Note that the behavior of the valve is highly repeatable, as shown by the small deviation between 500 cycles overlaid in Figure 1H, even for the dynamics that occur during the unstable transitions. Moreover, we find that for this specific design of the valve, the cycle frequency can be tuned in a range between $f \approx 0.3$ and 5 Hz by varying the inflow rate from $Q_{in} = 0.2$ to 4.5 SLPM (and up to $f \approx 17$ Hz by minimizing the capacitance $C_0$ by removing the flow sensor), as shown in Figure S1. For higher values of inflow, the valve stops oscillating and remains open. Details on the durability of the valve obtained by performing an experiment lasting 10 h are shown in Figure S2.

To explain the oscillating behavior, we make use of the analogy between fluidics and electronics, in which pressure can be described by a voltage and fluid flow by a

Please cite this article in press as: van Laake et al., A fluidic relaxation oscillator for reprogrammable sequential actuation in soft robots, Matter (2022), https://doi.org/10.1016/j.matt.2022.06.002



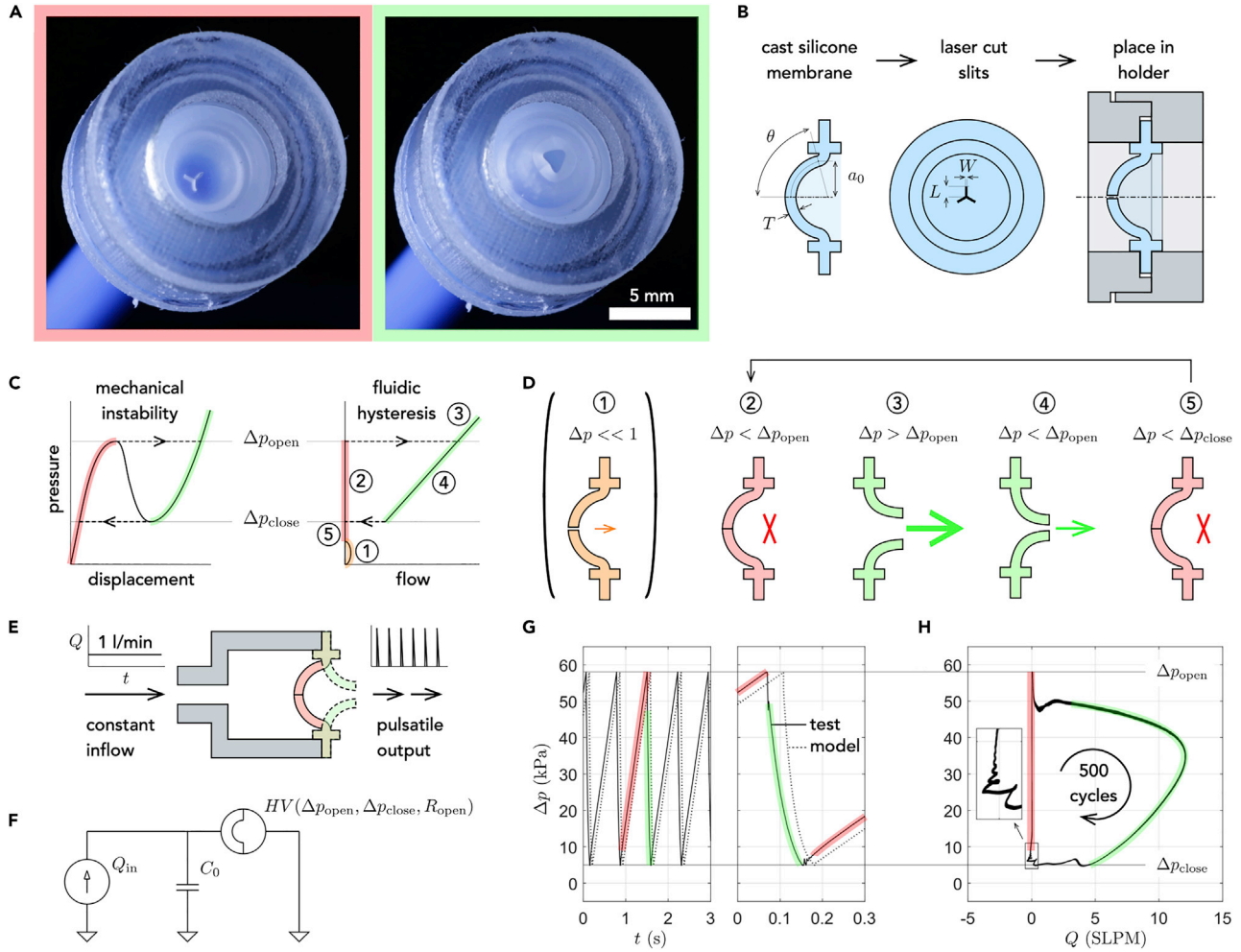


**Figure 1. A hysteretic valve that transforms a continuous flow into a pulsatile flow**

(A) Experimental realization of a hysteretic valve in its initially closed (red) and buckled open (green) states.

(B) Design and parameters of the valve.

(C and D) Schematic of the underlying hysteresis in the nonlinear behavior between the pressure, displacement, and effective flow through the valve (C), as a result of the various states the valve can be in (D).

(E and F) Schematic of the experimental setup that translates a continuous flow into a pulsatile flow (E), which can be modeled using the electronic analogy (F).

(G) Measured (solid) and simulated (dashed) pressure drop $\Delta p$ over the valve in response to a continuous inflow of $Q$ = 1 SLPM.

(H) Relation between the measured pressure drop $\Delta p$ over the valve and flow rate $Q$ through the valve, for 500 cycles (cycle 100 to 600) overlaid. Red and green highlights represent closed and open states of the valve.

current[30] (Figure 1F; experimental procedures). Using this analogy, we model the hysteretic valve as a voltage-controlled switch with a resistance $R_{open}$ and $R_{closed} \gg R_{open}$ in its open and closed states (note that our definition of open is opposite to electronics and indicates that air can flow through the valve), respectively. Moreover, we model the combined deformation of the valve and compressibility of the air contained in the tubes before the valve as a capacitor $C_0$. This provides the energy storage that is required for the system to oscillate. To simulate constant inflow, we drive the system with a current source. This circuit then forms a fluidic relaxation oscillator, characterized by the periodic, relatively slow build up and fast release of pressure. Note that in electronics, the same effect can be witnessed in a Pearson-Anson oscillator,[31] where a neon tube provides the required hysteresis. This also explains why the valve stops oscillating at higher flow rates,

Please cite this article in press as: van Laake et al., A fluidic relaxation oscillator for reprogrammable sequential actuation in soft robots, Matter (2022), https://doi.org/10.1016/j.matt.2022.06.002





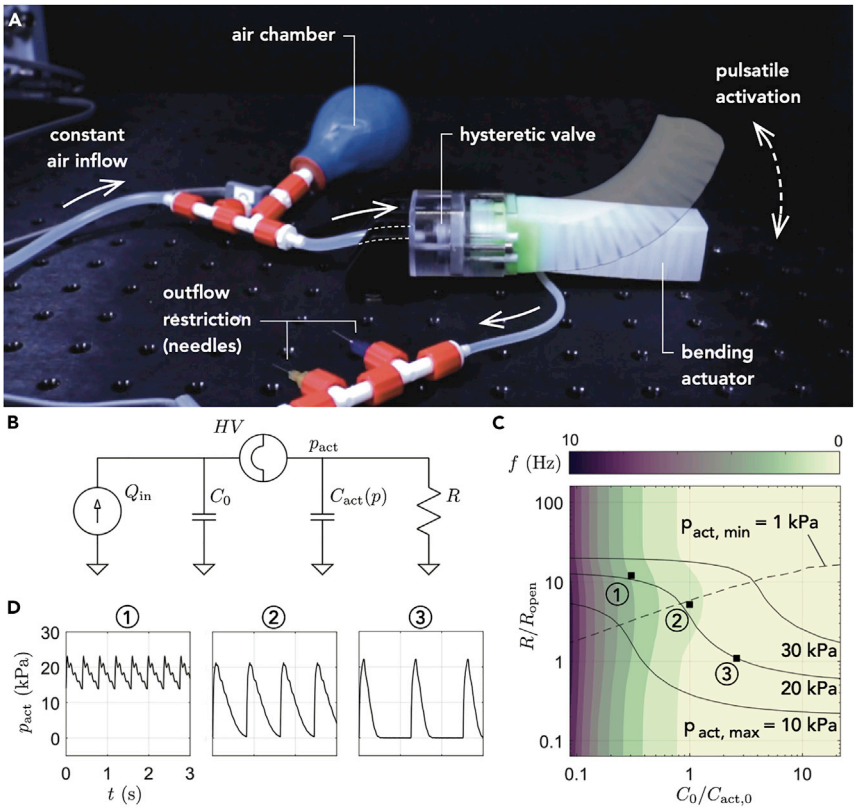


**Figure 2. Cyclic activation of a single actuator using a hysteretic valve**

(A) Experimental setup with a bending actuator directly connected to a hysteretic valve, where an additional air chamber is placed before the valve and an outflow restriction after the actuator.

(B) Equivalent electronic circuit of the experimental fluidic circuit.

(C) Simulated cycle frequency and actuator pressure as function of outflow restriction $R$ and capacitance of the air chamber $C_0$, for fixed flow rate $Q_{in}$ = 1 SLPM. The solid lines indicate the peak actuator pressure at $p_{act,max}$ = 10, 20, and 30 kPa, and the dashed line indicates the minimum actuator pressure at $p_{act,min}$ = 1 kPa.

(D) Actuator pressure $p_{act}$ obtained in three experiments to exemplify the potential behavior of the fluidic circuit, where we have used $Q_{in}$ = 1 SLPM and $\{C_0/C_{act,0}, R/R_{open}\}$ = $\{0.3, 12.0\}$, $\{1.0, 5.2\}$, $\{2.6, 1.1\}$, corresponding to markers ①, ②, and ③ in (C), respectively. In the experiments, the secondary oscillations are caused by mechanical vibrations of the actuator.

as the pressure difference caused by the drag force of the constant flow prevents the valve from snapping back.

These three components (current source, capacitor, and hysteretic switch) are enough to accurately capture the oscillating response of the system, as can be seen in Figure 1G from the comparison between our model and experiments. Note that, here, we always use air in our fluidic circuits, such that a fixed volume acts as a capacitance through the compressibility of the air. However, the same results could be obtained using, for example, water, although in that case an elastic chamber is required to achieve capacitance. Moreover, we should also note that in our simulations, we did not model the dynamic effects that are visible in Figures 1G and 1H during valve opening and closing. This does not affect the descriptive power of the model since the effective time scales are sufficiently separated.

Please cite this article in press as: van Laake et al., A fluidic relaxation oscillator for reprogrammable sequential actuation in soft robots, Matter (2022), https://doi.org/10.1016/j.matt.2022.06.002



### Cyclic activation of a single actuator

Next, we couple our fluidic relaxation oscillator to a soft bending actuator to achieve cyclic activation (Figure 2A; Video S2). We fabricate a modified PneuNet actuator based on a design that was previously used in an untethered soft robot,[2,32] where we limit the required amount of air to inflate the actuator[33] (Figure S3). To integrate the actuator with the hysteretic valve, we use a 3D-printed clamp to hold the valve and actuator in place and to connect the valve to an inflow. The actuator has an outflow port to which we connect a silicone tube. We furthermore connect an air chamber in front of the valve to be able to vary the volume of air that will be compressed prior to each actuation ($C_0$) and add one or more needles to act as a flow restriction ($R$) after the outflow tube to reduce the rate at which the air leaves the actuator while being vented to atmosphere (Figure 2A).

To determine the circuit parameters that are needed to achieve a desired motion profile of the actuator (i.e., maximum and minimum pressure and cycle frequency), we first perform a numerical study by considering the equivalent electronic schematic as shown in Figure 2B (experimental procedures). Given a specific (nonlinear) pressure volume relation of the actuator (Figure S3) and the parameters of our hysteretic valve, we can still choose the flow rate ($Q_{in}$), size of the air chamber ($C_0$), and the outflow restriction ($R$). For example, Figure 2C shows the resulting activation frequency $f$ of the actuator when varying $C_0$ (normalized by the initial actuator capacitance $C_{act,0}$) and $R$ (normalized by the hysteretic valve resistance $R_{open}$) for a constant inflow of $Q_{in}$ = 1 SLPM. The same analysis is shown in Figure S4 for a range of flow rates.

While these results show that we can tune the frequency of activation, different combinations of $C_0$ and $R$ lead to different actuator pressurization. To illustrate this, we consider all possible parameter combinations that lead to a maximum pressure in the actuator $p_{act,max}$ = 20 kPa, as indicated by the line in Figure 2C. We choose this value as it is high enough to achieve significant deformation of the actuators but does not cause excessive fatigue. Along this line, we can identify two regimes. At low outflow resistance $R$ (i.e., higher $C_0$), deflation of the actuator occurs more rapidly than inflation of the air chamber, such that the actuator empties completely before being activated again. Therefore, it is at zero pressure for part of the cycle (Figure 2D, case 3). In contrast, at high outflow resistance $R$ (i.e., lower $C_0$), the inflation of the air chamber is initially faster than the deflation of the actuator. Therefore, a new equilibrium is found where $p_{act,min} > 0$, such that the actuator no longer goes back to its undeformed shape (Figure 2D, case 1). At the boundary of these two regimes, we find the actuator to always be in motion while still fully deflating during each cycle. The dashed line in Figure 2C approximates this boundary for different values of $p_{act,max}$, where we have set the minimum pressure in the actuator equal to $p_{act,min}$ = 1 kPa. We can now identify the unique combination of parameters $\{C_0/C_{act,0}, R/R_{open}\}$ that leads to $p_{act,max}$ = 20 kPa and $p_{act,min}$ = 1 kPa for $Q_{in}$ = 1 SLPM (Figure 2D, case 2).

### Alternating activation of two actuators

A typical soft robot contains multiple actuators that need to be activated in a certain pattern to achieve a desired behavior, such as locomotion. In order to determine if we can use our hysteretic valve to control fluidic circuits that contain more than one actuator, we next focus on fluidic circuits that contain two actuators. While it is straightforward to achieve simultaneous activation of any number of actuators by connecting them all to a single valve, it is not directly obvious how we can achieve alternating activation. To achieve this, we place two identical valves in parallel and

Please cite this article in press as: van Laake et al., A fluidic relaxation oscillator for reprogrammable sequential actuation in soft robots, Matter (2022), https://doi.org/10.1016/j.matt.2022.06.002





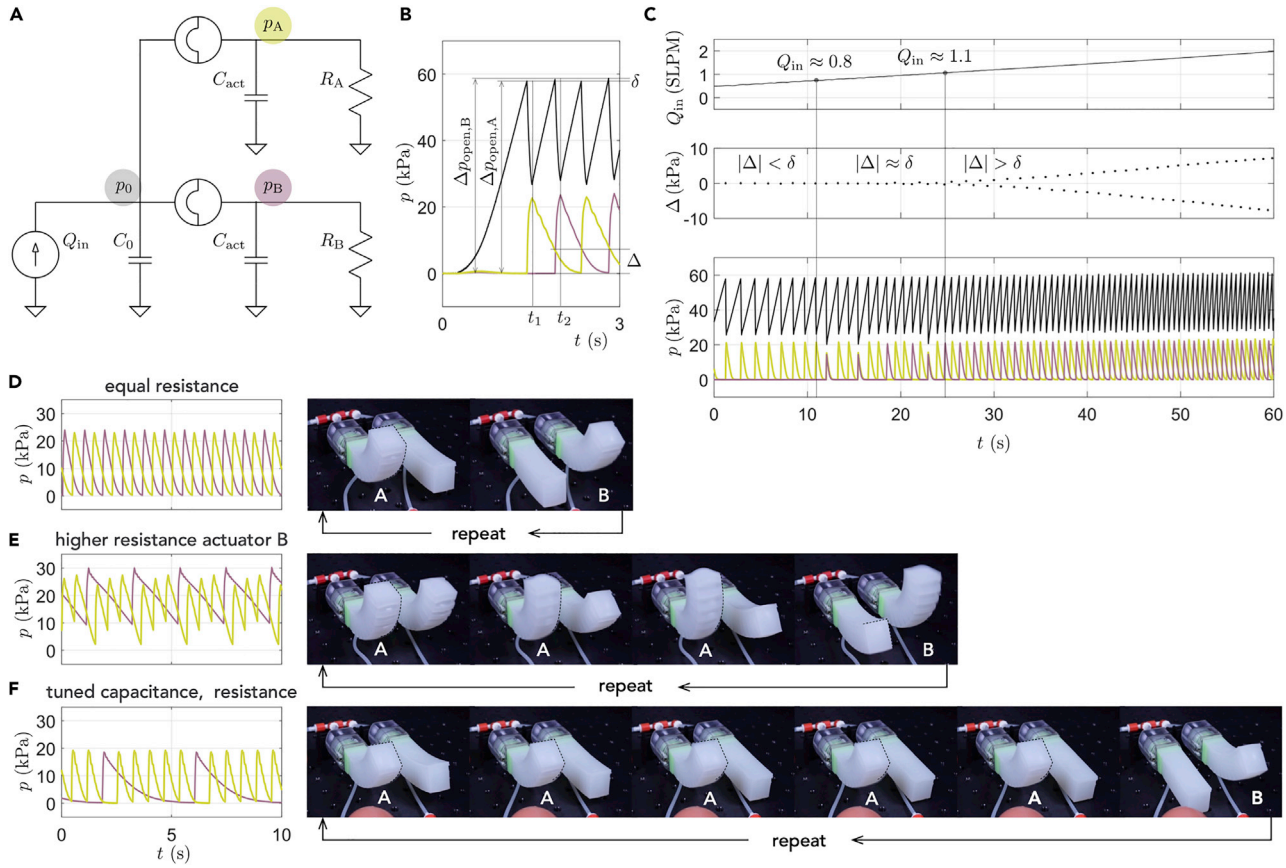


**Figure 3. Alternating activation of two actuators using two hysteretic valves placed in parallel**

(A) Equivalent electronic circuit of the experimental setup.

(B) Measured pressures in the air chamber (black line) and actuators (yellow and purple lines) for $Q_{in}$ = 2 SLPM, starting from atmospheric pressure.

(C) Experimentally measured pressures for a sweep of $Q_{in}$ = 0.5 to 2 SLPM in 60 s.

(D) Nearly identical actuators and valves result in a 1:1 activation of actuators A (yellow) and B (purple), as indicated by the measured pressure and still images of the experiment.

(E and F) Different ratios can be obtained by varying the fluidic components, for example, by (E) increasing $R_B$ to obtain a 3:1 activation ratio or (F) precisely tuning $C_0$, $C_B$, and $R_B$ to obtain a 5:1 activation ratio.

connect them to a single air chamber, as shown in the schematic in Figure 3A. Excitingly, when applying a constant flow of $Q_{in}$ = 2 SLPM to this fluidic circuit, the actuators spontaneously start to activate in anti-phase (Figures 3B and 3D; Video S3).

To better understand this behavior, we first look at pressure $p_0$ in air chamber $C_0$ placed upstream and pressures $p_A$ and $p_B$ in the two actuators A and B (Figure 3B). Starting from the situation where the complete fluidic circuit is at atmospheric pressure, initial inflation causes $C_0$ to start charging, compressing the air inside the chamber, such that $p_0$ increases. When, at $t = t_1$, pressure in the upstream air chamber reaches $p_0 = \Delta p_{open}$, both valves feel the same pressure difference $\Delta p_A = \Delta p_B = \Delta p_{open}$. Now, in the idealized symmetric schematic, both valves should open, such that both actuators are activated simultaneously. However, this behavior is unstable, and any imperfection will cause one valve to reach its critical pressure first. Specifically, we observe that a small imperfection δ exists between the critical pressures of valves A and B, such that $\Delta p_{open,A} = \Delta p_{open,B} - \delta$, where $\delta > 0$. This imperfection causes valve A to open before valve B. As a result, valve B remains

Please cite this article in press as: van Laake et al., A fluidic relaxation oscillator for reprogrammable sequential actuation in soft robots, Matter (2022), https://doi.org/10.1016/j.matt.2022.06.002



closed since the upstream pressure $p_0$ drops immediately after valve A opens. The second time that the pressure $p_0$ in the upstream air chamber reaches $p_0 = \Delta p_{open}$, at $t = t_2$, actuator A has not fully deflated yet. Therefore, valve A feels a lower pressure difference than valve B such that, this time, valve B opens instead. It is important to note that this sequential activation of the actuators requires that the pressure difference between actuators at the moment one of the valves opens, $\Delta$, is greater than the imperfection between the valves $\Delta > \delta$. Also note that sequential actuation does not rely on the small manufacturing differences between the valves. On the contrary, zero imperfection would always result in $\Delta > \delta$. The experimentally observed imperfection does, however, cause the alternating mode to be initiated immediately, where in the theoretical case of perfectly identical valves, it would take a small external disturbance to enter it. This is analogous to, for example, symmetry breaking observed in beam buckling.

To study the range of parameters for which $\Delta > \delta$ in more detail, we perform an experiment where we sweep the inflow rate $Q_{in}$ from 0.5 to 2 SLPM in 60 s (Figure 3C). Firstly, we find that for $Q_{in} < 0.8$ SLPM, only actuator A gets activated. In our experiment $\Delta p_{open,A} < \Delta p_{open,B}$ and at these flow rates, actuator A has sufficient time to empty before being activated again, such that $\Delta < \delta$. Secondly, when $Q_{in} > 1.1$ SLPM, we find that A and B alternate since there is sufficient pressure difference between the valves (i.e., $\Delta > \delta$). Interestingly, in between these regimes (when $\Delta \approx \delta$), a transition occurs, where the actuators are activated in seemingly erratic patterns. To better understand this regime, we perform an additional experiment where we sweep the flow rate more slowly from 0.2 to 2 SLPM in 8 h (Figure S5). Here, we find for $0.45 \leq Q_{in} \leq 1.2$ SLPM a finite activation ratio that varies from $A{:}B = 7{:}1$ to 1:1 via a range of intermediate values. An unexpected observation is that actuators A and B regularly activate simultaneously throughout this erratic regime. In the idealized schematic, this can only happen if at that moment $p_A - p_B = \delta$. However, clearly, this condition can never be met precisely. Therefore, we believe that there must be a higher-order effect such as a weak coupling between the valves that causes them to synchronize. For this work, we did not explore the nature of this coupling effect further, as we can avoid it by choosing parameters that result in a sufficiently large pressure margin $\Delta$.

While alternating activation (i.e., 1:1) is robustly achievable for a wide range of flow rates $Q_{in} > 1.2$ SLPM, the results from Figure 3C show that simply setting the flow rate does not allow us to robustly vary the activation ratio. Instead, we can achieve this by varying the individual deflation times of the two actuators by varying the components that comprise the fluidic circuit. For example, the deflation time can be increased by increasing $R$ or $C_{act}$. As a first demonstration, we change the outflow restriction after actuator B, resulting in an activation ratio of 3:1 (Figure 3E). However, increasing $R_B$ also increases both the minimum and maximum pressures in actuator B, as can be expected based on the analysis shown in Figure 2C. As such, by selecting appropriate values for both $C_{act}$ and $R$, we can set the activation ratio as well as the maximum pressure for both actuators. Here, as an example, we show that we achieve a 5:1 activation ratio at equal maximum pressures by a rational selection of $Q_{in}$, $C_0$, $C_{act,B}$, and $R_B$ (experimental procedures).

### Scaling the number of valves and actuators

Having discovered an instability that leads to two actuators being activated in sequence, a natural question to ask is if we can robustly control the activation sequence for more than two actuators using this effect. Recall that for two actuators, we only see stable cycling when the pressure difference at activation $\Delta$ is greater

Please cite this article in press as: van Laake et al., A fluidic relaxation oscillator for reprogrammable sequential actuation in soft robots, Matter (2022), https://doi.org/10.1016/j.matt.2022.06.002





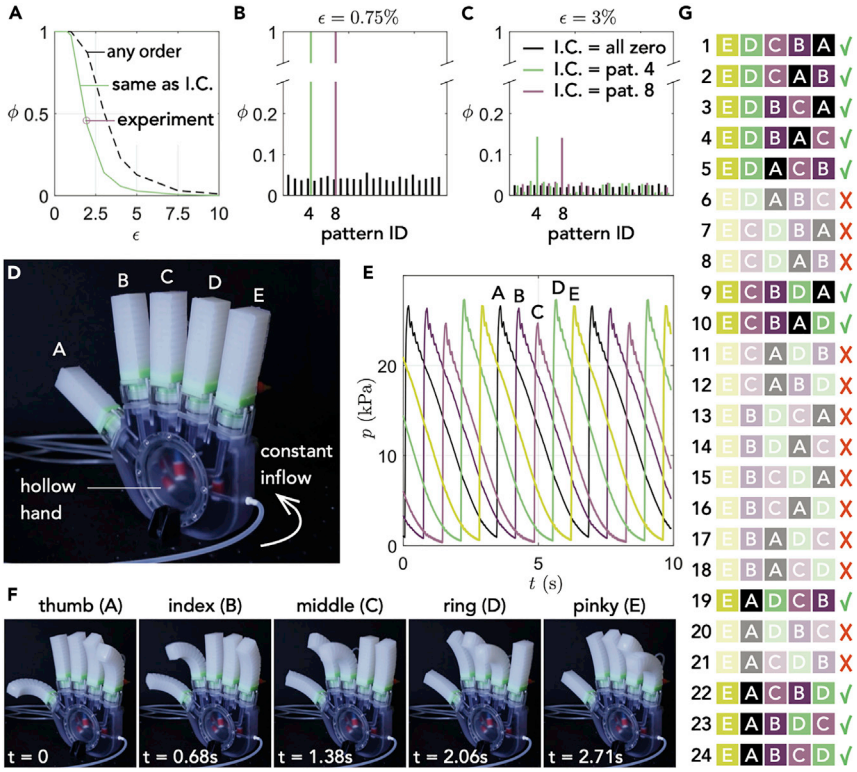


**Figure 4. Potential activation sequences for a fluidic circuit consisting of five valves and actuators placed in parallel**

(A) The dashed black line indicates the fraction φ of simulations at a relative imperfection ε that result in a stable sequence that involves all five actuators, each exactly once, when starting from atmospheric pressure. The solid green line indicates the fraction of a different set of simulations, where the resulting sequence corresponds to the initial pressures set separately in each actuator (I.C., initial conditions).

(B and C) Fraction of the simulations that result in a specific pattern (ID = 1 to 24) for $\varepsilon = 0.75\%$ (B) and $\varepsilon = 3\%$ (C). The black bars indicate the simulations that start from atmospheric pressure, while the green and purple lines indicate simulations where the initial pressures correspond to two different sequences (patterns 4 and 8 respectively; see G).

(D) Experimental realization of a robotic hand with five soft bending actuators and valves and an air chamber embedded in the hand palm.

(E and F) Measured pressure for $Q_{in} = 2.5$ SLPM when starting from atmospheric pressure (E), illustrated by still images of the experiment at specific times (F).

(G) Initial conditions that we applied corresponding to pattern ID = 1 to 24. Green checkmarks (red crosses) indicate that the corresponding sequence was (not) observed.

than the imperfection δ. Since Δ decreases with the number of actuators (Figure S6), we expect that the number of actuators that we can control in sequence is limited by imperfections. Such imperfections could, for example, be the result of production tolerances or variations in the environment.

To study the effect of such imperfections on the sequential behavior, we focus on a fluidic circuit with five actuators and valves in parallel and perform a Monte-Carlo analysis. To do so, we create sets of valve parameters by multiplying each valve parameter (i.e., $\Delta p_{open}$, $\Delta p_{close}$, and $R_{open}$) by a relative imperfection drawn from a uniform distribution $[1 - \varepsilon, 1 + \varepsilon]$. For a range of imperfections $0.005 \leq \varepsilon \leq 0.1$ ($0.5\% \leq \varepsilon \leq 10\%$), we perform 3,000 simulations where all actuators start from atmospheric pressure. Interestingly, from the results shown in Figure 4A, we observe that for imperfection values $\varepsilon \leq 1\%$, all simulations result in stable sequences involving all

Please cite this article in press as: van Laake et al., A fluidic relaxation oscillator for reprogrammable sequential actuation in soft robots, Matter (2022), https://doi.org/10.1016/j.matt.2022.06.002



five actuators, each exactly once. This can be seen from the ratio φ (Figure 4A, dashed line), which indicates the fraction of simulations that results in a stable sequence that involves all actuators. For larger imperfections, we find $\varphi < 1$, indicating that some sequences involve less than five actuators, up to the limit for which $\varphi \approx 0$ at $\varepsilon \approx 10\%$, where in each sequence there is always at least one actuator that is not being activated, or some of the actuators activate multiple times.

So far, we have counted the fraction of stable sequences for any activation order. However, there are a total of $N!/N$ unique periodic patterns that involve all $N$ actuators (i.e., 24 for five actuators). By inspecting the distribution of patterns that we find for two selected imperfection levels (0.75% and 3%), we find that there is an equal probability for each pattern to occur when all actuators start from atmospheric pressure (Figures 4B and 4C, black bars). However, for most practical applications, we would want to be able to select a specific sequence. To achieve this, we next explore if it is possible to use different initial conditions to initiate each of the 24 available patterns. When we apply a specific pattern of initial pressure levels in the actuators, we expect them to activate in order of increasing initial pressure, as the valve whose actuator has the lowest initial pressure will reach its critical pressure difference for opening first.

To verify this approach of setting initial conditions, we perform 200 Monte Carlo simulations for each imperfection level and for each of the 24 initial conditions corresponding to every unique order of activation. Figure 4A shows the fraction of runs that result in stable sequencing in the same order as the initial pressure applied to the actuators or, equivalently, the fraction of the 24 available orders we can select on average. Excitingly, we find that for small $\varepsilon \leq 0.75\%$, we can reliably initiate any of the 24 patterns. However, for $0.75\% < \varepsilon \leq 4\%$, the number of achievable patterns decreases rapidly until, for $\varepsilon > 4\%$, it drops below 1 pattern on average ($\varphi < 1/24 = 0.04$). The effect that imperfection has on the stability of the sequence is further exemplified in Figures 4B and 4C, where we show results obtained by repeating the Monte Carlo simulations for two specific initial conditions 3,000 times, and we observe that for an imperfection level of $\varepsilon = 3\%$ only 15% ($\varphi = 0.15$) of all simulations result in the same pattern as the initial condition. Still, these results show that by applying initial conditions we can control the activation sequence, with better specificity at lower imperfection levels.

To verify these findings experimentally, we produce a robotic hand demonstrator with five soft bending actuators. All actuators are connected in parallel to a shared hollow palm that acts as the fluidic capacitor. The outflow of each actuator is restricted by a needle (Figure S7). Between each actuator and the palm, we insert one of our soft hysteretic valves (Figure 4D), which we select from a larger batch to have similar parameters (experimental procedures). In an initial experiment, we increase the inflow rate until we witness sequential activation of all fingers. The flow rate at which this happens, as well as the resulting frequency and maximum and minimum actuator pressures, depends on the size of the hollow palm and the outflow restriction. For the setup as shown in Figures 4D and S7 (needle diameter 0.33 mm, $C_0$ = 0.5 mL/kPa), we observe robust sequencing at $Q_{in}$ = 1.75 SLPM, for which $f_{cycle}$ = 1.5 Hz, $p_{act,max}$ = 26 kPa, and $p_{act,min}$ = 1 kPa (Figures 4D–4F; Video S4).

To sample how many other patterns can be achieved by applying different initial conditions, we reduce the maximum actuator pressure to ensure that the actuators will not tear after prolonged use. We increase the needle diameter to 0.41 mm and

Please cite this article in press as: van Laake et al., A fluidic relaxation oscillator for reprogrammable sequential actuation in soft robots, Matter (2022), https://doi.org/10.1016/j.matt.2022.06.002





use a smaller $C_0$ = 0.25 mL/kPa. For this setup, stable activation starts at $Q_{in}$ = 2.5 SLPM, for which $f_{cycle}$ = 3.4 Hz, $p_{act,max}$ = 22 kPa, and $p_{act,min}$ = 2 kPa. We then vary the initial conditions (experimental procedures; Video S4) and find that we can initiate 11 stable sequences (Figure 4G), i.e., $\varphi = 11/24 = 0.46$. We then approximate the imperfection level by comparing the opening pressure difference for the five valves (Figure S8), and we find $\varepsilon = 1.9\%$. When comparing the experimentally realized value of $\varphi$ with the results from our Monte-Carlo analysis for the same value of $\varepsilon$, we see that the two closely match (Figure 4A). This leads us to believe that by improving the production tolerances on the valve and other components, we should be able to obtain all sequences or even scale to more then five valves. Yet, in practical applications, it may be beneficial to actually limit the number of existing patterns to those that the application requires, such as two or three different gaits in a multi-legged robot. To achieve this, one could select or create valves and actuators with different behavior (i.e., selecting or designing them to have larger imperfections instead of smaller).

### Physically reprogramming the sequence of activation

Having demonstrated the capability to program different sequences in the same hardware configuration by setting the initial conditions, we now demonstrate a method to physically reprogram the order of activation during operation in a setup with three actuators and valves (Figure 5; Video S5). Starting from a stable C-B-A sequence (Figure 5A), we briefly block the venting of actuator C starting just after the next actuator (B) has been activated. We hold it while A is activated and release it immediately when actuator B has been activated a second time (Figure 5B). This puts actuator C first in line after B, reversing the order from C-B-A to A-B-C (Figure 5C). Crucially, the activation of actuator C is not simply offset by the exact duration of blocking. Instead, the system finds a new equilibrium that is not affected by the details of the temporary disturbance. Note that the timing does not have to be exact, and there is a specific allowed window for both the blocking and release moments that depends on the frequency (Figure S9). This allows us to routinely change the order back and forth (Video S5). Moreover, the method is not fundamentally limited to three actuators. For example, it is possible to switch from one stable sequence to another in our hand demonstrator (Video S6). However, for five actuators, multiple steps may be required to reach a specific sequence, and it would be beneficial to reduce the number of existing sequences to improve the physical reprogrammability. Finally, these results also indicate that other (significant) disturbances might reverse the order as well, which could be particularly interesting for sensing and feedback control.

### A walking robot with embedded hysteretic valves

To study the feasibility of using our fluidic relaxation oscillators under more realistic conditions, we embed a fluidic circuit into a four-legged mobile robot (Figures 6A; experimental procedures; Video S7). Here, we focus on robustness under nonideal inflow conditions, as well as dynamic actuator loading, rather than focusing on the ideal walking sequence or physical reprogrammability.

The robot consists of four bending actuators that are connected to a 3D-printed rigid body with embedded air chamber. The air chamber has an inlet to which we attach an off-the-shelf membrane pump (NMP850KPDC-B, KNF). The pump is not placed on the robot because of its weight (360 g) but is connected via a silicone tube. The two front legs are connected to the air chamber in parallel, where we place a hysteretic valve between each leg and the central body. Their outflow is restricted with identical needles (diameter 0.51 mm). Of the two back legs, only the left actuator is

Please cite this article in press as: van Laake et al., A fluidic relaxation oscillator for reprogrammable sequential actuation in soft robots, Matter (2022), https://doi.org/10.1016/j.matt.2022.06.002



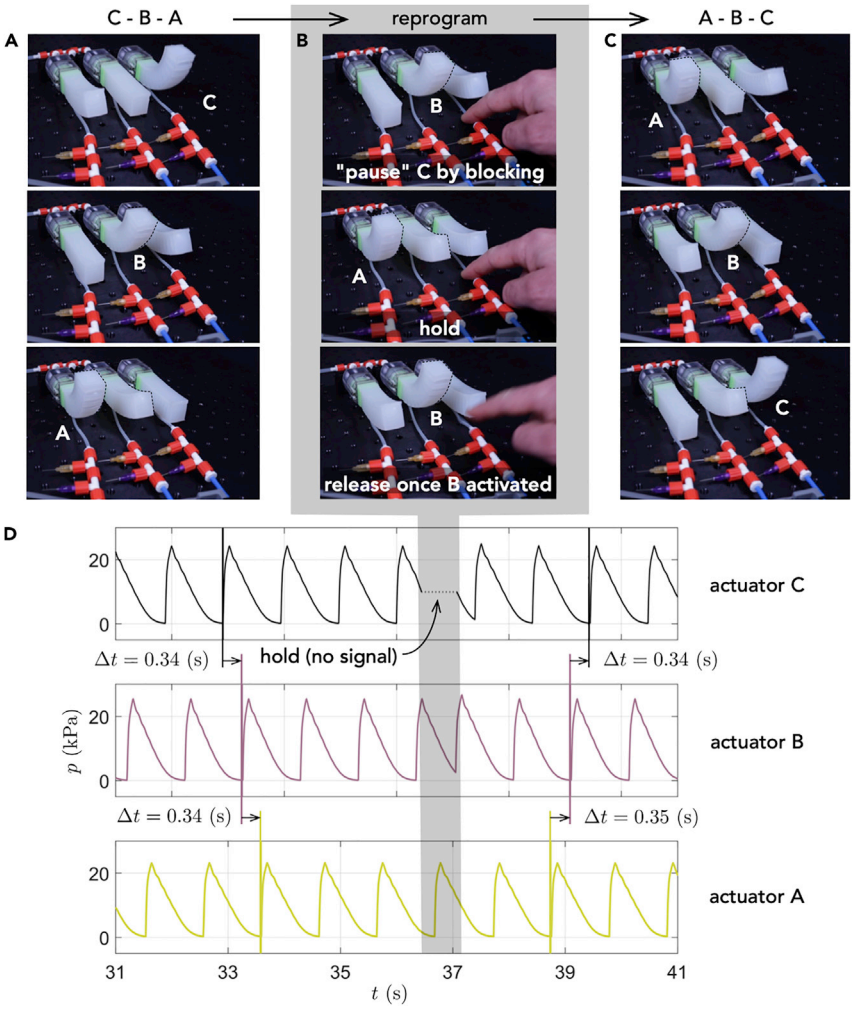


**Figure 5. Physically reprogramming a sequence in a fluidic circuit consisting of three parallel valves and actuators**

(A–C) The fluidic circuit (A) initially activates at stable sequence C-B-A, which is (B) reprogrammed by temporarily blocking the outflow of actuator C, switching to (C) a new stable sequence A-B-C. (D) Measured pressure in the three actuators for the same experiment, where we have used $Q_{in}$ = 3 SLPM. Note that during blocking of the exhaust, the pressure in actuator C is not recorded, as the sensor is placed behind the flexible tube used for blocking the flow. $\Delta t$ marks the time delays between consecutive activations.

connected to the air chamber via a hysteretic valve. The other is mechanically connected, but air flow to and from the air chamber is blocked. Instead, the back legs are coupled by a tube to enable simultaneous activation. The outflow from these combined actuators is restricted by a narrower needle (diameter 0.2 mm). As a result of a final fine-tuning step, we place an additional external air chamber on top of the robot body in order to increase the maximum actuator pressures upon activation, which is needed for the actuators to carry the weight of the robot. The equivalent electronic circuit is shown in Figure 6B.

We next turn on the pump, operating at constant motor speed (30 Hz), and observe the resulting actuation sequence (Figures 6C–6L). The front legs alternate with a 1:1 ratio, as expected based on results from a circuit with two valves and actuators with identical outflow restrictions (Figure 3D). The back legs activate less frequently,

Please cite this article in press as: van Laake et al., A fluidic relaxation oscillator for reprogrammable sequential actuation in soft robots, Matter (2022), https://doi.org/10.1016/j.matt.2022.06.002





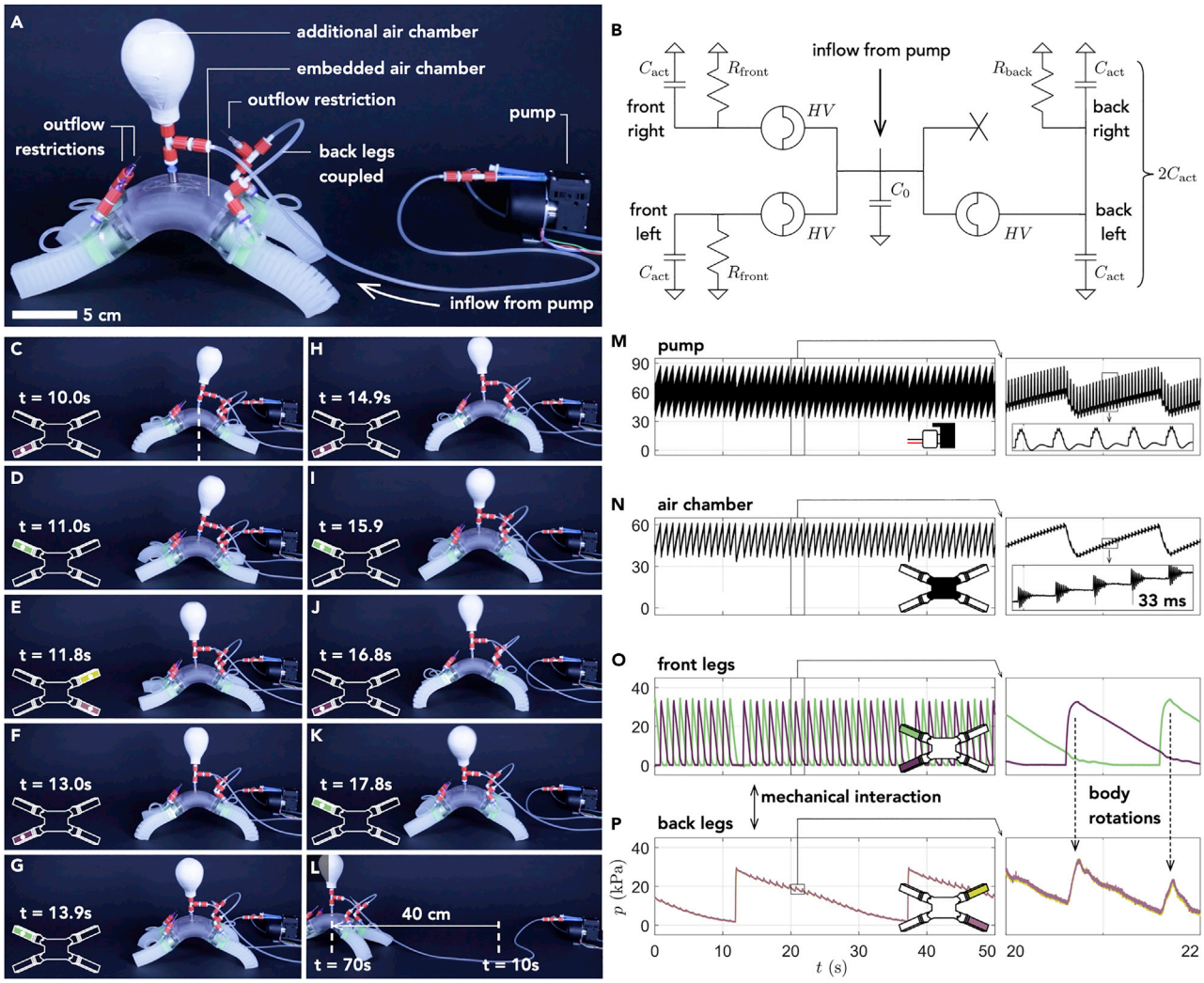


**Figure 6. A walking robot with embedded hysteretic valves**

(A) Overview of the robot and membrane pump. Scale bar is 5 cm.

(B) Equivalent electronic circuit.

(C–L) Overview of the walking sequence, showing key valve activation steps (Video S7). Initially, the front legs alternate (C and D). At $t$ = 11.8 s, the back legs are activated (E). After that, the front legs alternate again, while the back legs slowly deflate (F–K). In 1 min (from $t$ = 10 to 70 s), the robot walks approximately 40 cm (L).

(M–P) Pressure traces recorded in an identical experiment. The pressures are measured (M) near the pump, (N) in the air chamber, (O) in both front legs, and (P) in both back legs. Right set of panels are enlarged views of the left panels.

which is a result of the narrower outflow restriction, while the maximum actuator pressure is similar to the front legs due to the doubled capacitance. This circuit demonstrates the possibility of combining the results for *N*:1 activation (Figure 3F) and 1:1 activation (Figure 3D) into a *N*:*N*:1 pattern.

In an identical experiment, we measure the pressure near the pump, as well as in the air chamber and all actuators, while the robot is walking (Figures 6M–6P). This reveals two important real-world considerations. First, the air flow provided by the membrane pump is highly pulsatile, as evidenced by the pressure pulses near the pump (Figure 6M) and the stepwise increase and oscillations of the pressure in the air chamber (Figure 6N). Second, the back legs show a periodic increase in pressure, synchronized with the activation

Please cite this article in press as: van Laake et al., A fluidic relaxation oscillator for reprogrammable sequential actuation in soft robots, Matter (2022), https://doi.org/10.1016/j.matt.2022.06.002



of the front legs (Figures 6O and 6P). This coupling is due to rotations of the robot upon activation of one of the front legs, causing dynamic variations of the weight distribution, which result in varying external forces on the actuators. Taken together, the walking robot demonstrates the feasibility of our fluidic circuits under more realistic conditions such as nonideal inflow conditions as well as dynamic loading.

## DISCUSSION

In this article, we present a soft and compact hysteretic valve and demonstrate its use in fluidic circuits to transform a continuous flow into cyclic pulses. Supported by a model that describes the dynamics of networks including one or more hysteretic valves, we experimentally demonstrate sequential motion of up to five actuators and physical reprogramming of the order of sequential activation in response to external stimuli in a network with three actuators. Finally, we show the feasibility of real-world task performance by embedding a fluidic circuit inside a four-legged mobile robot. This work focuses on the behavior of various fluidic circuits, which are all made using the exact same valve design. In future work, we will study how the elastic behavior of the valve can be tuned to achieve different opening and closing pressures by changing, for example, the curvature, thickness, slit pattern, or material.

One important finding is that although there is a potential to activate a different number of actuators by using valves in parallel, imperfections set a practical limit to the number of actuators that can be activated in sequence. In this work, we produce valves using methods such as 3D printing and laser cutting. Improved repeatability could potentially be achieved by industrial production methods. Another potential avenue is to reduce the effect that imperfections have on the system by shaping the (nonlinear) pressure-volume behavior of the actuators. For example, a linear decay of the pressure in the actuator shows a considerably lower sensitivity to imperfections compared with an exponential decay (Figure S6).

While in all our experiments, we use a rigid holder to clamp the valves, the holder does not have to be rigid. To demonstrate this, we also build a soft container that we introduce as an additional casting step. It should be noted that the soft container does affect the quantitative behavior of the valve (not qualitative), as it introduces a dependency on the absolute pressure. This dependency originates from the expansion of the soft container due to the internal pressure, such that for higher internal pressure the valve is slightly stretched. This stretching reduces the opening and closing pressure difference (Figure S10).

Our work could find direct practical implementation in the bio-medical field[34] or control of responsive mobile robots aimed at exploration in harsh environments, with a possibility to even expand their capabilities to autonomous sensing. Here, we already demonstrate the effectiveness of complete blocking of an outflow as a mode of interaction with the environment, but we envision that a variety of other feedback mechanisms could be added to the circuits, including the incorporation of elements that change their fluidic capacitance and resistance as a function of external inputs. Such elements could be used to directly alter the oscillating frequency of an actuator.

Recently, attention for electronics-free actuation and control of soft robots has grown.[35–39] Equivalents of basic building blocks of digital control, such as logic gates, are being re-invented in the fluidic domain. As a result, we also see basic

Please cite this article in press as: van Laake et al., A fluidic relaxation oscillator for reprogrammable sequential actuation in soft robots, Matter (2022), https://doi.org/10.1016/j.matt.2022.06.002





higher-level functions emerge, such as analog to digital converters, memory, and state machines. In digital electronics, circuits are based on very simple elements, and advanced higher-level functionality is achieved only by densely integrating as many of them as possible in a small space. However, in fluidics, the circuit behavior depends on scale as viscous forces become increasingly important at smaller scales, such that there is a limit to how small the proposed fluidic components and circuits can be made, and thus there is a limit to the functionality of the fluidic control far from the current state of the art in digital electronics. As such, in contrast to electronics, we believe that in fluidic control of soft robots, there is a need for components with highly nonlinear behavior, where we harness physical principles to embody intelligent behavior in circuits with a limited number of components. Importantly, the nonlinear behavior of the hysteretic valve presented in this work showcases the potential to maintain simple designs for the fluidic elements yet achieve complex controllable and reprogramable behaviors.

## EXPERIMENTAL PROCEDURES

### Resource availability

#### *Lead contact*

Further information and requests for resources and materials should be directed to and will be fulfilled by the lead contact, Johannes T.B. Overvelde (overvelde@amolf.nl).

#### *Materials availability*

This study did not generate new unique reagents.

#### *Data and code availability*

The experimental and numerical data that support the findings of this study and all computer algorithms necessary to run the models have been deposited at Zenodo (doi: 10.5281/zenodo.6576063).

### Fabrication of valves

The valves are produced by injecting a silicone elastomer pre-polymer (Dragon Skin 20, Smooth-On) in a 3D-printed mold (Eden260VS, Stratasys). We print molds using VeroClear for model material and Sup707 for support. After printing, we post-process the molds by mechanically removing most support material using a high-pressure waterjet, followed by soaking in 5% KOH solution for 24 h. We brush off any remaining residue under a running water tap using a toothbrush then dry the molds for 5 h at 40°C. We spray the molds lightly with mold release (Ease Release 200, Mann).

Before casting the silicone rubbers, the pre-polymer components (A and B, Dragon Skin 20, Smooth-On) are thoroughly stirred individually then separately poured in the two compartments of a syringe (MIXPAC AF 400-01-10-01, Siko B.V.). The syringe with unmixed components is degassed using vacuum. After degassing, the plungers are placed, and the syringe is fitted with a static mixer (MFQ 05-24L) and conical needle (20 Gauge, Metcal 920125-DH) and placed in a pneumatically driven dispenser (MIXPAC DP 400-85). The mold is first injected from one opening, where we should note that a single bubble systematically forms near the exit opening. Directly after this first injection, we inject pre-polymer a second time from the other side (the exit opening), which reliably drags the bubble with it and out from the mold through the first opening, leaving the mold perfectly filled. Note that we keep an uninterrupted flow from the dispenser throughout the filling process, as we observe some bubble formation in the mixture upon starting of the extrusion.

Please cite this article in press as: van Laake et al., A fluidic relaxation oscillator for reprogrammable sequential actuation in soft robots, Matter (2022), https://doi.org/10.1016/j.matt.2022.06.002



After the 4 h curing process, the membrane is removed from the mold, and three slits are laser machined at its apex (Speedy 300, Trotec). To ensure proper alignment during the laser cutting, we create a custom holder on the same machine by first cutting a circular hole of diameter $D$ = 8 mm from a polymethylmethacrylate (PMMA) sheet (6 mm thickness). We then place the valve with its rim in this holder. The individual slits have length $L$ = 0.75 mm, and the width resulting from laser machining varies from $W$ = 25 μm on the convex side where the laser enters to $W$ = 5 μm on the concave side. The valve holders used to clamp valves during experiments are directly 3D printed using the same 3D printer, material, and post-processing step. A complete overview of the fabrication steps is given in Figure S11.

### Fabrication of actuators, a robotic hand, and a walking robot

A similar casting procedure is used to fabricate the soft bending actuators (Figure S12). To fabricate these components, we use a softer silicone elastomer (Dragon Skin 10 Medium, Smooth-On). All mold parts are 3D printed (VeroClear, Eden260VS, Stratasys) except for the plates that separate the air chambers. These plates are laser machined from polyoxymethylene (POM) sheets (0.5 mm thickness).

In a first casting step, the top (containing the chambers) and bottom parts are cast in separate molds. The mold for the top part has an integrated angled stand, and pre-polymer is injected from an inlet near the bottom to avoid air entrapment. Moreover, sufficient pre-polymer is injected to also fill an overflow reservoir located on top of the mold. This reservoir connects to the mold cavity via a series of small holes and serves to provide pre-polymer to fill voids that are created during subsequent degassing (for 10 min in vacuum). In this first casting step, a silicone tube (inside diameter [ID] = 1.5 mm, outside diameter [OD] = 3 mm) is integrated into the top part. The interface is abraded with sandpaper and cleaned with isopropanol to promote adhesion.

To be able to connect the soft actuator to a rigid clamp, we integrate a connection part from stiffer silicone elastomer (Elite Double 32, Zhermack) in a second casting step that we perform 4 h after the first casting step. After another 20 min, we remove the top part with the integrated connection part from its mold and connect it to the bottom part using Dragon Skin 10 Very Fast (Smooth-On). In this step, we integrate a strain-limiting layer between the top and bottom parts. The strain-limiting layer consists of a laser-cut Mylar mesh with thickness 100 μm. Note that the timing of the casting steps is important to ensure a good connection between the different silicone rubbers.

The integrated connection part can be connected directly to a 3D-printed clamp containing the valve. Similarly, five actuators with integrated valve can be connected to a 3D-printed palm to construct a robotic hand (Figure S13), and four actuators can be connected to a 3D-printed robot body to build a walking robot (Figure S14). Note that prior to assembling the robotic hand, we measure the response of a total of 20 valves in a separate experiment (similar to the experiment depicted in Figures 1 and S1) to select five valves. Focusing on $\Delta p_{open}$, we cluster the valves in groups of increasing size, minimizing for $\delta = \Delta p_{open,max} - \Delta p_{open,min}$ (Figure S15). We use three of those five valves for the mobile robot.

### Fluidic circuits and experiments

Fluidic circuits are assembled from the fabricated valves and actuators, pressure chambers, and flow resistances (precision dispensing needles, TE-series, Metcal). In order to easily assemble different circuits using the same components, we use

Please cite this article in press as: van Laake et al., A fluidic relaxation oscillator for reprogrammable sequential actuation in soft robots, Matter (2022), https://doi.org/10.1016/j.matt.2022.06.002





male, female, and "T" Luer-Lock connectors (MLRL, FTL, LT, Nordson Medical). The flow input is provided by a mass flow controller (SLA5850, Brooks Instrument).

We use differential pressure sensors (MPX5100DP, NXP), in-line pressure sensors (26PCDFG5G, Honeywell), and thermal mass flow sensors (AWM510xVN, Honeywell) to characterize the pressures and flows in the fluidic circuits. To control the experiments and data acquisition, we use a USB-powered I/O device (NI-DAQ USB-6212, National Instruments) and custom software. Note that in order to perform reliable high-frequency measurements using the USB-6212, we connect one of the analog inputs to ground, and we configure the device such that it samples the dummy input between any two real measurements. This prevents cross-talk between inputs via the parasitic capacitance of the analog to digital converter, which is significant if this precaution is not taken.

### Tuning the activation ratio for two actuators

In order to achieve a 5:1 ratio in an experiment with two nearly identical actuators and valves placed in parallel (Figure 3F), we follow an experimental approach that is guided by our numerical analysis. We start by varying the needles to achieve $R_B > R_A$, in order to obtain different relaxation times, as this is the basis for an activation ratio different from 1:1. Next, we can extract from Figure 2C that an equal maximum actuator pressure can be maintained by increasing $C_{act,B}$, such that $C_{act,B} > C_{act,A}$. However, for an activation ratio of 5:1, the faster actuator (A) will effectively receive most (5/6) of the flow, while the slowed-down actuator (B) receives the rest. Given a total inflow of 2 SLPM, this means that approximately 1.7 SLPM will flow through actuator A. From Figure S4, we then find that the faster actuator will equilibrate at a higher pressure (similar to Figure 3E where we only changed one of the needles to increase $R_B$). To avoid this increase of the minimum actuator pressure for actuator A, we lower the flow rate, while at the same time, we decrease $C_0$ to keep the cycle frequency constant. In practice, at this stage, we applied a final fine-tuning of $C_B$ until we achieved equal maximum pressure.

### Applying initial conditions

In the experiments where we apply different initial pressures, we use a single pressure regulator (15.5 kPa) and a custom pressure divider (Figures S16 and S17). The pressure divider is constructed from five silicone tubes (SFM3-1550, Trelleborg, 0.64 mm inside diameter) that are connected in series by using a 22G needle (ID = 0.41 mm, OD = 0.72 mm) on both ends of each tube. The used tube lengths are 65, 65, 40, 8, and 14 cm, resulting in pressures of approximately 15.5, 12, 7, 3.5, and 2 kPa, respectively, after each additional stage of the pressure divider. These values correspond to mean pressure levels just before one of the valves opens during stable cyclic activation. The bending actuators' outflow tubes are manually connected to one of the pressures to provide the specific initial pressures for each experiment.

To run each experiment, a pressure regulator is connected in parallel to the mass flow controller that is flowing into the hollow palm of the hand demonstrator. Initially, both are activated, with set points $p_0$ = 50 kPa and $Q_{in}$ = 2.5 SLPM, respectively. Once the set-point pressure is reached, the pressure regulator starts sinking the air input, keeping the pressure constant. The pressure $p_0$ = 50 kPa is selected to ensure all valves remain closed due to sufficient positive pressure difference, even if initial pressure is applied to the bending actuators. Next, to initiate the sequential activation, the pressure regulator is isolated from the hand, such that it no longer sinks the inflow provided by the mass flow controller, and the pressure

Please cite this article in press as: van Laake et al., A fluidic relaxation oscillator for reprogrammable sequential actuation in soft robots, Matter (2022), https://doi.org/10.1016/j.matt.2022.06.002



**Table 1. Fluidic-electronic equivalence**

| Electronic | | | | Fluidic | | |
|---|---|---|---|---|---|---|
| Voltage | $V$ | (V) | ↔ | pressure | $p$ | (kPa) |
| Current | $I$ | (A) | ↔ | flow rate | $Q$ | (mL/s) |
| Charge | $Q$ | (C) | ↔ | volume | $V$ | (mL) |
| Resistance | $R$ | (Ω) | ↔ | restriction | $R$ | (kPa/(mL/s)) |
| Capacitance | $C$ | (F) | ↔ | capacitance | $C$ | (mL/kPa) |

in $C_0$ starts to rise. At the same time, the bending actuators are disconnected from their initial pressures and connected to their outflow restrictions. Note that this syncing is done manually, such that there is a deviation in the exact timing between experiments. Therefore, we attempt the same initial condition up to three times.

## Numerical model

To simulate our fluidic circuits, we make use of the freeware circuit simulator LTspice, which specializes in simulating electronic circuits with switching components. We make use of the analogy between electronic and fluidic circuits (Table 1). Although the analogy between electronics and fluidics is very useful, there are some differences that need to be taken into account when using software originally made to simulate electronic circuits. Most of these differences can be circumvented, which we try to exemplify below using two of the main components.

(1) Capacitance in electronics is defined as the change in stored charge per unit change in electrical potential, i.e., $C = dQ/dV$. According to the fluidic-electronic analogy, fluidic capacitance is then the change in volume of medium stored per unit change in pressure difference, $dV/d\Delta p$. However, if we take volume to be the geometrical volume, this does not hold for compressible media such as air. This can be seen when we try to model the inflation of a fixed volume, which would have zero capacitance, since $dV = 0$ by definition. This is correct when using an incompressible fluid, but not for for a compressible fluid. We circumvent this issue by noting all volumes (and flow rates) as "standard" volumes (and flow rates), meaning the volume an amount of gas would have if it were at a reference pressure. Assuming constant temperature, standard volume is essentially a unit of mass rather than volume. Using standard volume, a fixed (geometrical) volume has a constant nonzero capacitance $dV_{standard}/d\Delta p$ that correctly models the compressibility of the medium. Using standard volumes has the additional advantage that we can directly use readouts from our flow rate sensors and controllers, as they also operate in SLPM.

(2) Typical fluidic restrictions (i.e., narrow tubes) have an almost quadratic relation between fluidic mass flow rate and pressure drop, while standard electronic resistors are assumed to be linear. However, the effect on main simulation output is minor, and we assume all resistors to be linear.

We model the valve as a voltage-controlled switch (component S). This component has hysteresis implemented as a standard feature, defined using a trigger voltage Vt and a peak-to-peak hysteresis Vh around Vt. Since our valve is placed in line, the switched and control grounds are always connected together, as well as the switched and control positive voltages. For ease of use, we create a custom symbol that exposes only these two combined terminals, and we define Vt=(Vopen + Vclose)/2 and Vh=(Vopen - Vclose)/2, allowing us to use the more convenient parameters $\Delta p_{open}$ and $\Delta p_{close}$.

The bending actuator is modeled as a nonlinear capacitor. We define a custom charge-voltage $Q(V)$ (volume-pressure $V(p)$) relation. The air chambers as well as other parasitic capacitance existing in, for example, the tubes are modeled as linear capacitors with a single parameter. Moreover, we model all restrictions as linear resistors $R$. All components are separately measured in the experimental setup, for example, as shown by the fit to the measured response of our soft actuators (Figure S3). As an example, Figure S18 shows the schematic used to simulate the results shown in Figure 2C.

Finally, note that for parametric studies, we use the command .STEP in LTspice, and we read data into MATLAB for processing. For Monte-Carlo analyses (Figure 4), we use the built-in function mc in LTspice to randomly vary parameter values, and we use MATLAB to write input files to LTspice for different initial conditions and imperfection levels as well as to process data.

## SUPPLEMENTAL INFORMATION

Supplemental information can be found online at https://doi.org/10.1016/j.matt.2022.06.002.

## ACKNOWLEDGMENTS

This project has received funding from the European Union's Horizon 2020 research and innovation program under grant agreement no. 767195. This work is part of the Dutch Research Council (NWO) and was performed at the research institute AMOLF.

## AUTHOR CONTRIBUTIONS

Conceptualization, L.C.v.L. and J.T.B.O.; methodology, L.C.v.L. and J.T.B.O.; software, L.C.v.L.; formal analysis, L.C.v.L. and J.T.B.O.; investigation, L.C.v.L., J.d.V., and S.M.K.; writing – original draft, L.C.v.L. and J.T.B.O.; writing – review & editing, L.C.v.L. and J.T.B.O.; visualization, L.C.v.L.; supervision, J.T.B.O.; funding acquisition, J.T.B.O.

## DECLARATION OF INTERESTS

The authors declare no competing interests.

Received: November 24, 2021
Revised: March 9, 2022
Accepted: May 31, 2022
Published: June 22, 2022

## REFERENCES

1. Bao, G., Fang, H., Chen, L., Wan, Y., Xu, F., Yang, Q., and Zhang, L. (2018). Soft robotics: academic insights and perspectives through bibliometric analysis. Soft Robot. *5*, 229–241. https://doi.org/10.1089/soro.2017.0135.

2. Tolley, M.T., Shepherd, R.F., Mosadegh, B., Galloway, K.C., Wehner, M., Karpelson, M., Wood, R.J., and Whitesides, G.M. (2014). A resilient, untethered soft robot. Soft Robot. *1*, 213–223. https://doi.org/10.1089/soro.2014.0008.

3. Shintake, J., Cacucciolo, V., Floreano, D., and Shea, H. (2018). Soft robotic grippers. Adv. Mater. *30*, 1707035. https://doi.org/10.1002/adma.201707035.

4. Polygerinos, P., Wang, Z., Galloway, K.C., Wood, R.J., and Walsh, C.J. (2015). Soft robotic glove for combined assistance and at-home rehabilitation. Robot. Auton. Syst. *73*, 135–143. https://doi.org/10.1016/j.robot.2014.08.014.

5. Payne, C.J., Wamala, I., Abah, C., Thalhofer, T., Saeed, M., Bautista-Salinas, D., Horvath, M.A., Vasilyev, N.V., Roche, E.T., Pigula, F.A., and Walsh, C.J. (2017). An implantable extracardiac soft robotic device for the failing heart: mechanical coupling and synchronization. Soft Robot. *4*, 241–250. https://doi.org/10.1089/soro.2016.0076.

6. Rus, D., and Tolley, M.T. (2015). Design, fabrication and control of soft robots. Nature *521*, 467–475. https://doi.org/10.1038/nature14543.

7. Suzumori, K., Iikura, S., and Tanaka, H. (1992). Applying a flexible microactuator to robotic mechanisms. IEEE Control Syst. *12*, 21–27. https://doi.org/10.1109/37.120448.

8. Shepherd, R.F., Ilievski, F., Choi, W., Morin, S.A., Stokes, A.A., Mazzeo, A.D., Chen, X., Wang, M., and Whitesides, G.M. (2011). Multigait soft robot. Proc. Natl. Acad. Sci. U S A *108*, 20400–20403. https://doi.org/10.1073/pnas.1116564108.

9. Marchese, A.D., Katzschmann, R.K., and Rus, D. (2015). A recipe for soft fluidic elastomer robots. Soft Robot. *2*, 7–25. https://doi.org/10.1089/soro.2014.0022.

10. Polygerinos, P., Correll, N., Morin, S.A., Mosadegh, B., Onal, C.D., Petersen, K., Cianchetti, M., Tolley, M.T., and Shepherd, R.F. (2017). Soft robotics: Review of fluid-driven intrinsically soft devices; manufacturing, sensing, control, and applications in human-robot interaction. Adv. Eng. Mater. *19*, 1700016. https://doi.org/10.1002/adem.201700016.

11. Gorissen, B., Reynaerts, D., Konishi, S., Yoshida, K., Kim, J.W., and De Volder, M. (2017). Elastic inflatable Actuators for soft robotic applications. Adv. Mater. *29*, 1604977. https://doi.org/10.1002/adma.201604977.

12. Bartlett, N.W., Tolley, M.T., Overvelde, J.T.B., Weaver, J.C., Mosadegh, B., Bertoldi, K., Whitesides, G.M., and Wood, R.J. (2015). A 3D-printed, functionally graded soft robot powered by combustion. Science *349*, 161–165. https://doi.org/10.1126/science.aab0129.

13. Katzschmann, R.K., DelPreto, J., MacCurdy, R., and Rus, D. (2018). Exploration of underwater life with an acoustically controlled soft robotic fish. Sci. Robot. *3*, eaar3449. https://doi.org/10.1126/SCIROBOTICS.AAR3449.

14. Marchese, A.D., Tedrake, R., and Rus, D. (2016). Dynamics and trajectory optimization for a soft spatial fluidic elastomer manipulator. Int. J. Robot Res. *35*, 1000–1019. https://doi.org/10.1177/0278364915587926.

15. Wehner, M., Truby, R.L., Fitzgerald, D.J., Mosadegh, B., Whitesides, G.M., Lewis, J.A., and Wood, R.J. (2016). An integrated design and fabrication strategy for entirely soft, autonomous robots. Nature *536*, 451–455. https://doi.org/10.1038/nature19100.

16. Drotman, D., Jadhav, S., Sharp, D., Chan, C., and Tolley, M.T. (2021). Electronics-free pneumatic circuits for controlling soft-legged robots. Sci. Robot. *6*, eaay2627. https://doi.org/10.1126/SCIROBOTICS.AAY2627.

17. Vasios, N., Gross, A.J., Soifer, S., Overvelde, J.T., and Bertoldi, K. (2020). Harnessing viscous flow to simplify the actuation of fluidic soft robots. Soft Robot. *7*, 1–9. https://doi.org/10.1089/soro.2018.0149.

18. Overvelde, J.T.B., Kloek, T., D'haen, J.J.A., Bertoldi, K., Jonas, J.A.D., and Bertoldi, K. (2015). Amplifying the response of soft actuators by harnessing snap-through instabilities. Proc. Natl. Acad. Sci. U.S.A. *112*, 10863–10868. https://doi.org/10.1073/pnas.1504947112.

19. Gorissen, B., Milana, E., Baeyens, A., Broeders, E., Christiaens, J., Collin, K., Reynaerts, D., and De Volder, M. (2019). Hardware sequencing of inflatable nonlinear actuators for autonomous soft robots. Adv. Mater. *31*, 1804598. https://doi.org/10.1002/adma.201804598.

20. Glozman, D., Hassidov, N., Senesh, M., and Shoham, M. (2010). A self-propelled inflatable earthworm-like endoscope actuated by single supply line. IEEE Trans. Biomed. Eng. *57*, 1264–1272. https://doi.org/10.1109/TBME.2010.2040617.

21. Ben-Haim, E., Salem, L., Or, Y., and Gat, A.D. (2020). Single-input control of multiple fluid-driven elastic actuators via interaction between bistability and viscosity. Soft Robot. *7*, 259–265. https://doi.org/10.1089/soro.2019.0060.

22. Napp, N., Araki, B., Tolley, M.T., Nagpal, R., and Wood, R.J. (2014). Simple passive valves for addressable pneumatic actuation. In Proc. - IEEE Int. Conf. Robot. Autom., pp. 1440–1445. https://doi.org/10.1109/ICRA.2014.6907041.

23. Mahon, S.T., Buchoux, A., Sayed, M.E., Teng, L., and Stokes, A.A. (2019). Soft robots for extreme environments: removing electronic control. In RobotSoft 2019 - 2019 IEEE Int. Conf. Soft Robot, pp. 782–787. https://doi.org/10.1109/ROBOSOFT.2019.8722755.

24. Bartlett, N.W., Becker, K.P., and Wood, R.J. (2020). A fluidic demultiplexer for controlling large arrays of soft actuators. Soft Matter *16*, 5871–5877. https://doi.org/10.1039/c9sm02502b.

25. Mosadegh, B., Kuo, C.H., Tung, Y.C., Torisawa, Y.S., Bersano-Begey, T., Tavana, H., and Takayama, S. (2010). Integrated elastomeric components for autonomous regulation of sequential and oscillatory flow switching in microfluidic devices. Nat. Phys. *6*, 433–437. https://doi.org/10.1038/nphys1637.

26. Preston, D.J., Rothemund, P., Jiang, H.J., Nemitz, M.P., Rawson, J., Suo, Z., and Whitesides, G.M. (2019). Digital logic for soft devices. Proc. Natl. Acad. Sci. U S A *116*, 7750–7759. https://doi.org/10.1073/pnas.1820672116.

27. Drotman, D., Jadhav, S., Karimi, M., Dezonia, P., and Tolley, M.T. (2017). 3D printed soft actuators for a legged robot capable of navigating unstructured terrain. In Proc. - IEEE Int. Conf. Robot. Autom., pp. 5532–5538. https://doi.org/10.1109/ICRA.2017.7989652.

28. Rothemund, P., Ainla, A., Belding, L., Preston, D.J., Kurihara, S., Suo, Z., and Whitesides, G.M. (2018). A soft, bistable valve for autonomous control of soft actuators. Sci. Robot. *3*, eaar7986. https://doi.org/10.1126/SCIROBOTICS.AAR7986.

29. Preston, D.J., Jiang, H.J., Sanchez, V., Rothemund, P., Rawson, J., Nemitz, M.P., Lee, W.K., Suo, Z., Walsh, C.J., and Whitesides, G.M. (2019). A soft ring oscillator. Sci. Robot. *4*, 1–10. https://doi.org/10.1126/scirobotics.aaw5496.

30. Oh, K.W., Lee, K., Ahn, B., and Furlani, E.P. (2012). Design of pressure-driven microfluidic networks using electric circuit analogy. Lab Chip *12*, 515–545. https://doi.org/10.1039/c2lc20799k.

31. Pearson, S.O., and Anson, H.S.G. (1921). The neon tube as a means of producing intermittent currents. Proc. Phys. Soc. Lond. *34*, 204–212. https://doi.org/10.1088/1478-7814/34/1/341.

32. Ilievski, F., Mazzeo, A.D., Shepherd, R.F., Chen, X., and Whitesides, G.M. (2011). Soft robotics for chemists. Angew. Chem. Int. Ed. *50*, 1890–1895. https://doi.org/10.1002/anie.201006464.

33. Mosadegh, B., Polygerinos, P., Keplinger, C., Wennstedt, S., Shepherd, R.F., Gupta, U., Shim, J., Bertoldi, K., Walsh, C.J., and Whitesides, G.M. (2014). Pneumatic networks for soft robotics that actuate rapidly. Adv. Funct. Mater. *24*, 2163–2170. https://doi.org/10.1002/adfm.201303288.

34. Cianchetti, M., Laschi, C., Menciassi, A., and Dario, P. (2018). Biomedical applications of soft robotics. Nat. Rev. Mater. *3*, 143–153. https://doi.org/10.1038/s41578-018-0022-y.

35. Pal, A., Restrepo, V., Goswami, D., and Martinez, R.V. (2021). Exploiting mechanical instabilities in soft robotics: control, sensing, and actuation. Adv. Mater. *33*, 2006939. https://doi.org/10.1002/adma.202006939.

36. McDonald, K., and Ranzani, T. (2021). Hardware methods for onboard control of fluidically actuated soft robots. Front. Robot. AI *8*, 720702. https://doi.org/10.3389/frobt.2021.720702.

37. Hoang, S., Karydis, K., Brisk, P., and Grover, W.H. (2021). A pneumatic random-access memory for controlling soft robots. PLoS One *16*, e0254524. https://doi.org/10.1371/journal.pone.0254524.

38. Hubbard, J.D., Acevedo, R., Edwards, K.M., Alsharhan, A.T., Wen, Z., Landry, J., Wang, K., Schaffer, S., and Sochol, R.D. (2021). Fully 3D-printed soft robots with integrated fluidic circuitry. Sci. Adv. *7*, eabe5257. https://doi.org/10.1126/sciadv.abe5257.

39. Song, S., Joshi, S., and Paik, J. (2021). CMOS-inspired complementary fluidic circuits for soft robots. Adv. Sci. *8*, 2100924. https://doi.org/10.1002/advs.202100924.